

Atomic and molecular emission spectroscopy measurements for characterization of laser-induced plasma dynamics

Christian G. Parigger*, Ghaneshwar Gautam, Alexander C. Woods, David M. Surmick and James O. Hornkohl

University of Tennessee Space Institute, Center for Laser Application, 411 B. H. Goethert Parkway, Tullahoma, TN 37388, USA.

ABSTRACT

This work discusses time-resolved measurements of atomic and diatomic spectra following laser-induced optical breakdown. Spatially- and temporally-resolved spectroscopy is employed to characterize micro-plasma generated in laboratory air. Stark-broadened atomic emission profiles for hydrogen alpha and beta are utilized to determine plasma characteristics for specific time delays. The plasma dynamics include: variations in Stark-broadening emission of hydrogen alpha and beta lines, occurrence of molecular spectra due to recombination radiation, and change in line shape and appearance of atomic and molecular spectra due to collision and plasma oscillations. Comparisons of electron densities determined from hydrogen alpha and nitrogen II lines allow one to evaluate hydrogen self-absorption effects within the laser-induced plasma. Of interest are laser ablation measurements of atomic and diatomic emission spectra from aluminium (Al), aluminium monoxide (AlO), titanium (Ti), titanium monoxide (TiO), and carbon Swan systems that can be readily observed in laser-induced plasma. Diatomic molecules are frequently encountered in combustion processes. Optical breakdown emission spectroscopy data usually include signatures of species such as nitric oxide (NO), hydroxyl (OH), and cyanogen (CN) that allow one to characterize air plasma. The experimental work comprises measurement and data analyses of diatomic molecular spectra combined with computations of accurate line-strengths

encompassing spectral superposition of both atomic and diatomic molecular species. Neodymium-doped yttrium (Nd:YAG) Q-switched, pulsed laser radiation is employed at the fundamental wavelength of 1064 nm to generate micro-plasma in air. A standard Czerny-Turner type spectrometer is used together with an intensified diode array detector or an intensified charge-coupled device to record spectra.

KEYWORDS: atomic spectroscopy, molecular spectroscopy, plasma diagnostic, laser ablation, time-resolved spectroscopy, laser-induced optical breakdown, laser spectroscopy, Balmer series, electron density, laser-induced plasma

1. INTRODUCTION

The generation of laser-induced plasma and subsequent spectroscopy studies of the radiating species have been a focus of research by various research groups in a substantial number of laboratories with interest in fundamental and applied Physics, as indicated in recently published books [1-6] and selected reviews and viewpoints [7-13]. Laboratory micro-plasma can be readily generated with pulsed laser radiation originating from a Q-switched Nd:YAG device. Pulse widths of several nanoseconds duration with peak irradiances above threshold for plasma generation can also facilitate further increase of the plasma due to absorption after achieving optical breakdown. Laser radiation with reasonable mode structure from Nd:YAG devices, with a pulse width of 10 nanosecond and energy per pulse of 100 mJ can provide 1 to 2

*Corresponding author: cparigge@tennessee.edu

orders of magnitude above threshold irradiance when focused into laboratory air with $f/4$ optics. The subsequent expansion in air follows the breakdown events that routinely can be induced at a repetition rate of 10 to 100 Hz, and it occurs at a speed on the order of a Mach number of $Ma \approx 100$, but is reduced to high hypersonic speed within the first 100 nanosecond after plasma generation. For a delay of about 1 microsecond, the expansion speed is supersonic at about Ma 3. In other words, the expansion speed is of the order of 1 mm per microsecond. Time resolved spectroscopy shows rich emission spectra and associated spatially- and temporally-depended dynamics, including formation of vortices that can be measured some 100 to 1000 microseconds after optical breakdown [12, 14-16]. In this work, we address recent measurements that aim to elucidate expansion phenomena associated with generation of micro-plasma in air and/or at surfaces, viz. laser ablation.

Laser-Induced Breakdown Spectroscopy (LIBS) is a subject of active research by a significant number of researchers all over the globe, including studies of material composition in Mars explorations. Recent interest in plasma dynamics includes use of ultra-short, amplified femtosecond laser radiation, and the study of the Physics associated with such short interaction times in femtosecond LIBS, or FLIBS, and laser-material interactions [17]. Noteworthy are several major international conferences annually or bi-annually that address Physics, Chemistry, and application of laser-generated micro-plasma [18, 19], for example, the recent 2014 LIBS conference in China, the 2013 Euro-Mediterranean Symposium on Laser Induced Breakdown Spectroscopy (EMSLIBS) meeting in Italy, and the recent 2014 Federation of Analytical Chemistry and Spectroscopy Societies (FACSS) or Science Exchange (SciX) meetings in the United States. Moreover, interest in laboratory plasma studies using laser-induced breakdown are also the focus of line shape conferences, e.g., the recent International Conference on Spectral Line Shapes (ICSLS) in Europe [20] and/or North America [21] with efforts of widening such conferences to other continents.

The usual understanding of micro-plasma generation with nanosecond laser pulses includes formation of plasma followed by laser heating. Ionization of air species occur, and free electron densities are

significantly high such that for example the hydrogen Balmer line in humid air cannot be observed until several hundred nanosecond after breakdown. Atoms or molecules excited to the higher energy levels can return to the lower levels by emitting radiation at the specific atomic transition or molecular band wavelengths. Typical work includes diagnostic applications of laser-induced plasma and associated dynamics to determine material composition. This is accomplished by evaluating wavelength and intensity of the atomic or molecular spectra; therefore, one can determine the type of an element and concentration of atoms in a sample. Laser Induced Breakdown Spectroscopy (LIBS) is now a valuable technique for analysis of elemental composition including the capability of the method to analyze solid, liquid and gases with no or little sample preparation, suitable for on-site analysis. LIBS applications of elemental analysis due to radiation from atomic spectra will be greatly increased by extending the study to measurements of molecular spectra, e.g., mid-infrared emissions in LIBS [22] or Laser Ablation Molecular Isotopic Spectrometry (LAMIS) [23].

Laser ablation and laser-induced plasma generation in gases employ laser radiation with energy per pulse on the order of tens to hundreds of mJ per pulse and focusing optics, viz. frequently a singlet lens. In laser-ablation, the plasma vaporizes a relatively small amount of the target material, typically commensurate with the size of focal volume, but usually the vaporized material is much smaller when using femtosecond radiation. The generated plasma contains ions, electrons, excited atoms and molecules formed by recombination or simply by breaking off molecules, e.g., carbon molecules in LIBS of graphene can occur as a result of breaking off such molecules.

In this work, a summary and review is presented of work that addresses emission spectroscopy of atomic and molecular species. Atomic hydrogen, especially the hydrogen Balmer series lines, characteristics, broadening, and shifts, and molecular fingerprints of selected diatomic molecules will be of interest, for instance: aluminium and aluminium monoxide, titanium and titanium monoxide, over and above diatomic molecules such as C_2 , OH, CN, NO, to name a few, and the associated approach in predicting and analyzing measured spectra [24-41].

As an application of atomic and molecular emission spectroscopy, the wavelength of the atomic spectral line allows one to identify the radiating element. The measured intensity of the emitted light allows one to infer the number of atoms of an element. Spatially- and temporally-resolved investigation of laser induced plasma, however, is desirable by use of Abel and/or Radon transforms [42], including consideration of electron impact ionization and dissociation that can become important [43]. Typical applications of molecular spectroscopy include identification, characterization of explosive combustion plumes, and study of stellar atmospheres and/or chemical composition [34, 44-47]. The LIBS technique shows important applications in biomedical research [48-51] encompassing other laser spectroscopy methods such as photo-acoustic spectroscopy. Selected examples include plasma formation in water, analysis of gallstone, *in situ* deciduous tooth, *in vivo* human nail studies, or tomography of dental tissue. Plasma generation in water is used to evaluate (i) threshold breakdown, (ii) plasma absorption coefficient and (iii) energy density, which are valuable information for laser surgery or angioplasty. Breakdown threshold research aims to determine the minimum achievable size of laser effect used for material processing or laser surgery. Measurements of plasma absorption coefficients allow one to determine the energy coupled and transmitted through the medium which is important for the safety of laser surgery near sensitive biological structure like retina. The plasma energy density determines mechanical effects like shock waves and cavitation as it is usually important to establish the potential and/or actual damage near the focused laser radiation [51].

2. MATERIALS AND METHODS

In many experimental studies, emission spectroscopy methods appear essential in the capture of the spectral signatures of atomic and diatomic molecules following generation of the micro-plasma. For example, the laser-induced optical breakdown plasma in gaseous hydrogen has been investigated with time-resolved emission spectroscopy, including determination of electron density and excitation temperature. Hydrogen Balmer series atomic lines like H_{α} , H_{β} , and H_{γ} are used to determine electron density and temperature. Specifically, H_{α} and H_{β} lines

can be used to determine electron density from Stark widths and shifts; H_{γ} and further members of the Balmer series may be utilized to infer electron excitation temperature applying the Boltzmann plot technique [12]. Red shifts and asymmetries can also be used to determine electron density [32]. Measured values of temperatures are slightly skewed by the background radiation and the high electron density. The recorded line intensities depend on the effect of self-absorption; therefore, a measurement of self-absorption is always an important part in experiments. The extent of self-absorption of the hydrogen Balmer alpha and beta lines can also be investigated for various time delays from plasma generation. Energy radiated by one of the atoms in an excited state may be absorbed by other atoms surrounded by it. Such atoms are coupled by the electromagnetic field and can radiate coherently. The probability of radiation absorption can be calculated from the equation of interaction of the atoms with the radiation. The absorbed energy may be lost due to emission of radiation at different frequency or due to collisions, see Ref. [52] for more details.

Figure 1 shows the typical experimental arrangement [28]. The Q-switched Nd:YAG laser (DCR-2A(10) PS; Quanta-Ray) is operated at the fundamental wavelength of 1064 nm, at a repetition rate of 10 Hz generating 13 ns, 190 mJ pulses. The laser beam is passed through a dichroic beam splitters to remove residual 532 nm components and to monitor the pulse-to-pulse variations. Three mirrors (NB1-K13; Thorlabs) are used to align the beam parallel to the spectrometer slit. The beam is focused to a spot size of 50 μm by using a coated quartz lens (SBX031; Newport) in laboratory air for optical breakdown and micro-plasma formation. The resulting micro-plasma is imaged onto the spectrometer slit by two quartz lenses (SPX049; Newport) where the last lens optically matches the spectrometer's f-number of 5.6. Gratings of 1200, 1800, or 3600 grooves/mm are selected to disperse the radiation from the plasma for various time-resolved spectroscopy studies with the 0.64 m spectrometer (HR640; Jobin-Yvon). The resulting spectra are collected and recorded with an intensified linear diode array and optical multichannel analyzer (OMA; 1460; EG&G Princeton Applied Research Corporation). In the study of the temporal phenomena of the

micro-plasma, a delay generator (DG535; Stanford) is used with various gate widths and time delays to trigger the OMA. Temporally resolved hydrogen Balmer series emission profiles can be measured by varying the time delay from optical breakdown. The spectra are recorded with an intensified linear diode array coupled to an Optical Multichannel Analyzer (OMA). The OMA is controlled with a delay and waveform generator to achieve temporally resolved measurements with the intensified, linear diode array. For the recording of spatially resolved images along the slit height, a 2-dimensional charged coupled device (ICCD; ANDOR Technology, model iStar) is used in place of the OMA and intensified linear diode array. For example, for a titanium sample, the ablation plume is imaged onto the slit of a spectrometer, equipped with an 1800 groove/mm grating that yields in typical setups a spectral resolution of 0.1 nm, by a singlet lens chosen to match the f-number of the spectrometer [28].

In a typical experiment, emission spectra from several optical breakdown events are recorded to increase signal-to-noise ratio. Synthetic spectra with different micro-plasma parameters are compared with experimental spectra. The fitting of the recorded and computed spectra is accomplished with a non-linear routine, viz. by use of the Nelder-Mead algorithm. Calculations usually include the spectral resolution to simulate the spectrometer-slit convolved spectra. Monte-Carlo simulation methods are utilized as a tool for error analysis. Standard calibration lamps like neon, mercury and hydrogen are used for wavelength calibration. Furthermore, the collected data or spectra are processed to include corrections for the detector's sensitivity and background. Subsequently, the experimental data are compared with computed spectra.

3. RESULTS

In general, the plasma radiation may be absorbed by the surrounding open air; it may also be absorbed by the outer edges of the plasma and cause extra broadening and distortion on line profiles. In this work, self-absorption effects due to the plasma will be discussed primarily with respect to the Balmer series. Plasma self-absorption can occur in principle. Without correcting for self-absorption, the electron density inferred from the broadening of the line will be larger than calculated from H_α . Self-absorption

typically affects measurements of line intensities, and it is related to the density of the emitting/absorbing species. This effect can be described by a self-absorption correction factor. This correction factor needs to be evaluated to determine the extent of self-absorption.

In the work discussed here, a duplicating mirror is introduced to evaluate the extent of plasma self-absorption. Radiation emitted from the plasma is imaged onto the spectrometer slit, but radiation to the adjacent side is retro-reflected as well using a mirror and a lens. The results obtained with and without the mirror are compared to determine the extent of self absorption. Figure 2 shows the comparison of recorded data with and without a duplicating mirror. This comparison of electron density from hydrogen alpha emissions with ionized nitrogen lines allows us to investigate the level of self-absorption. The electron density can be determined from the H_α Stark broadening and shift [53-55], but it can equally be determined from ionized nitrogen N^+ lines for early time delays [56]. The H_α line is red-shifted from 656.28 nm, the N^+ lines are only slightly shifted from 648.21 nm and 661.06 nm [38, 56]. The electron density of 14 to $20 \times 10^{23} \text{ m}^{-3}$ determined from the H_α line is higher than 12 to $13 \times 10^{23} \text{ m}^{-3}$ obtained from N^+ for the 300 ns time delays. Therefore, H_α shows self-absorption for delays of 300 ns; however, the level of self-absorption is insignificant for delays of 800 ns after optical breakdown. The level of self-absorption is determined from addition of the mirror and comparison of continuum radiation and recorded emission line. Figure 3 illustrates results of the comparisons in the study of self-absorption effects with the duplication mirror [57]. The self-absorption by the plasma [57-61] is of interest, rather than the effects due to propagation through media beyond the plasma, as for example elaborated in nitric oxide (NO) self-absorption experiments [62].

In the analysis of the self-absorption experiments with the duplicating mirror, the correction factor [57] is evaluated using

$$K_\lambda = \frac{\ln\{y_\lambda\}}{y_\lambda - 1}, \quad y_\lambda = \frac{R_\lambda - 1}{R_C - 1}. \quad (1)$$

The continuum radiation ratio, R_C , and the signal ratio above the continuum, R_λ , is obtained from the

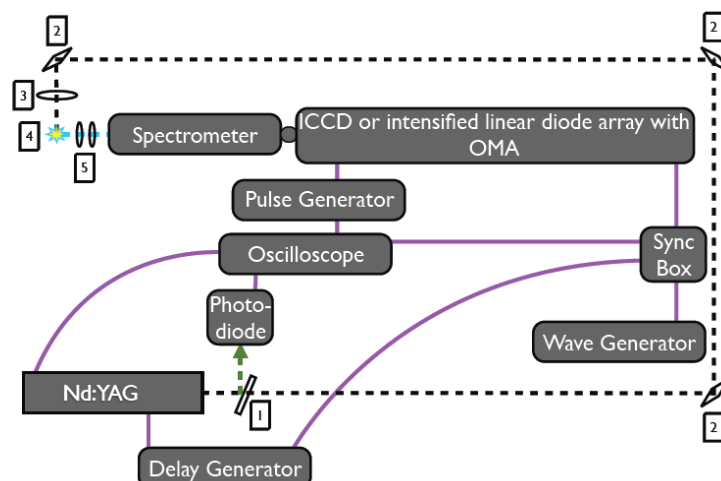


Figure 1. Experimental schematic for LIBS: (1) Beam splitter, (2) Mirrors, (3) Focusing lens, (4) Plasma, and (5) Focusing lenses. (Reproduced from Ref. [28] Parigger, C. G., Woods, A. C., Witte, M. J., Swafford, L. D. and Surmick, D. M. 2014, *J. Vis. Exp.*, 84, E51250, with permission from JoVE publication.)

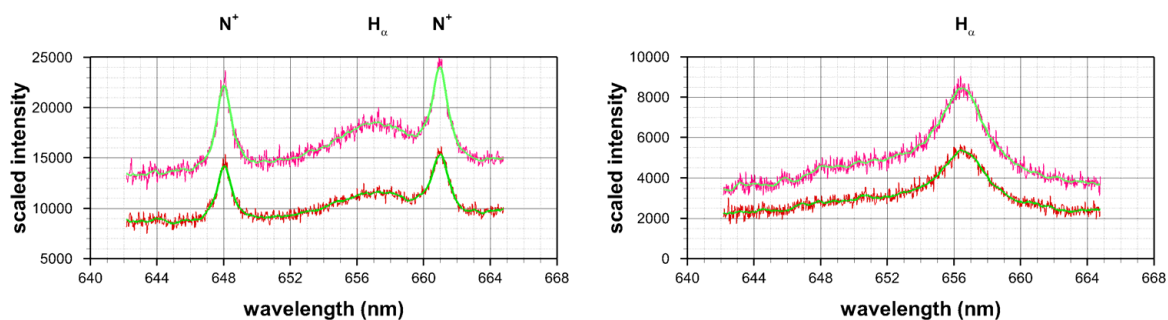


Figure 2. Comparison of spectra w/ and w/o mirror (**Left**) for 300 ns time delay, (**Right**) for 800 ns time delay. Slit height: 6.15 mm. The smoothed line shapes are Savitzky-Golay filtered.

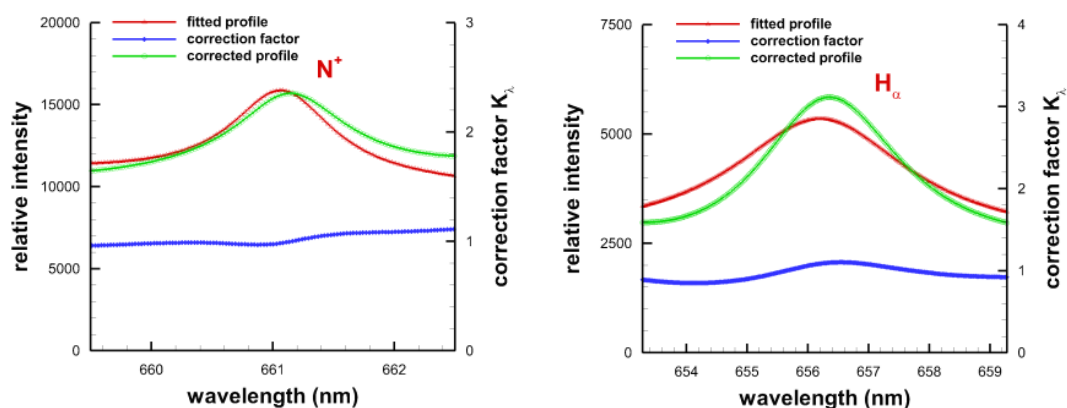


Figure 3. Corrected and fitted profile with correction factor. The fitted profile is obtained by determining the Lorentz profile from the experimental data. (**Left**) N^+ for a time delay of 300 ns, (**Right**) H_α for a time delay of 800 ns. Slit height: 6.15 mm.

recorded data with and without the mirror. In the analysis, it is important to establish whether indeed the nitrogen lines are possibly self-absorbed. The results for the 661.056 nm N^+ line indicate a correction factor of ≈ 1 , see Figure 3. The determination of the electron density from the N^+ line is deemed to be reliable in the interpretation of the 300 ns H_α data. The indicated formula for the 300 ns H_α data cannot be utilized due to difficulty in establishing the continuum ratio R_C . Evaluation of the correction factors for the 800 ns H_α data shows that self-absorption for such time delays is insignificant in optical breakdown studies in air. It is important to note that self-absorption investigations in laser-ablation experiments usually show the requirements for corrections.

Recent experimental records from laser-induced optical breakdown in air were collected using an intensified charge-coupled device (ICCD). Figure 4 illustrates the results for time delays of 300, 400, 700, and 800 ns. The complimentary images collected with the mirror in place served the purpose of evaluation self-absorption, compare Figure 2. The singly ionized nitrogen lines are clearly discernible on either side of the H_α line for the 300 ns data.

Experimental studies of diatomic molecular aluminium monoxide spectra is of interest in a variety of LIBS applications due to presence of aluminium in a variety of substrates that are investigated by generating laser-induced plasma. In addition, measurements of combustion phenomena that include aluminium usually result in strong signatures of AIO. The computation of diatomic line strength utilizes the so-called Wigner-Witmer eigenfunctions that permit significant simplifications in the implementation of selected rules by use of the Hönl-London factors, including accurate calculation of AIO line-strengths in the Hund case a basis, see Refs. [63, 64] that give details of the theoretical treatment and implementation. Figure 5 illustrates a computed molecular band using accurate line strengths, and it also shows typical experimental results. Figure 6 displays recorded and fitted AIO emission spectra following laser-induced optical breakdown in air.

Measurement of laser-ablation of titanium using time-resolved laser spectroscopy methods shows occurrence of ionized titanium lines during the

first few microseconds after optical breakdown [31, 41, 65, 66], followed by formation of TiO due to recombination of titanium with oxygen in air [67-69]. Spatially- and temporally-resolved imaging indicates the existence of a region forming a shell at the periphery of the plasma for which recombination processes producing TiO emissions begin to dominate over the collisional processes believed to dominate regions of primarily atomic spectral signatures [13, 36]. While recombination is considered the dominant process contributing to TiO emissions in laser ablation plasma, the disparity in the temperature inferred from the TiO spectral transitions emanating from just above the target's surface raises questions concerning the mechanisms contributing to the TiO emissions in this region. This particular laser-ablation effort has been the subject of an extensive study especially from the view point of pulsed laser deposition due to the wide ranging applications of TiO_2 thin films [70-80]. Figure 7 illustrates experimental results collected with an ICCD attached to the Czerny-Turner type JY680 spectrometer. Figure 7 also demonstrates localized TiO emissions along with Ti spectral emissions as recombination processes become predominant.

The computation of the spectra illustrated in Figures 5 to 7 follows the same approach, in principle, as previously communicated for selected diatomic molecules C_2 , CN, OH, NO, to name a few molecules of interest in plasma spectroscopy, in plume spectroscopy, in measurements of aerospace flows, e.g., see Ref. [81] and applications of emission spectroscopy with ultra-short, femtosecond laser pulses in combustion diagnostics, e.g., see Ref. [82].

The starting point for the computation of diatomic molecular spectra is usually the consideration of the so-called line strength

$$S_{ul} = \sum_u \sum_l |\langle u | T_k^{(q)} | l \rangle|^2. \quad (2)$$

Here, u and l indicate sums over the upper and lower states, respectively; $T_k^{(q)}$ is the operator (irreducible tensor operator) describing the optical transition. Evaluation of the diatomic line strength is further elaborated for the carbon *Swan* system in Ref. [64]. However, these line strengths are generated starting

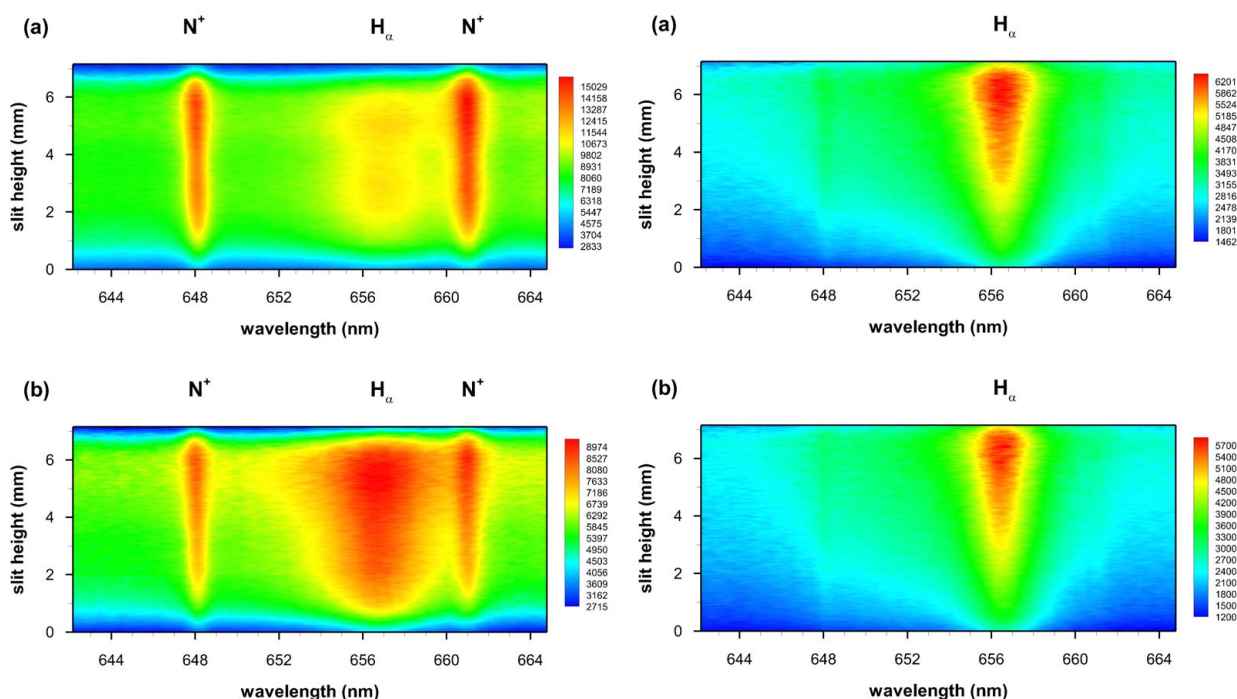


Figure 4. Left: (a) 300 ns; (b) 400 ns time delay. Right: (a) 700 ns; (b) 800 ns time delay. For the earlier time delays, the N⁺ lines allow one to determine electron density and evaluate H_α self-absorption. The nitrogen lines are hardly discernible for later time delays in the expanding micro-plasma. From the recorded images, a plasma expansion speed on the order of 300 to 100 μm in 100 ns can be determined, or 3 to 1 km/s, in the range of 0.3 to 1 μs after optical breakdown.

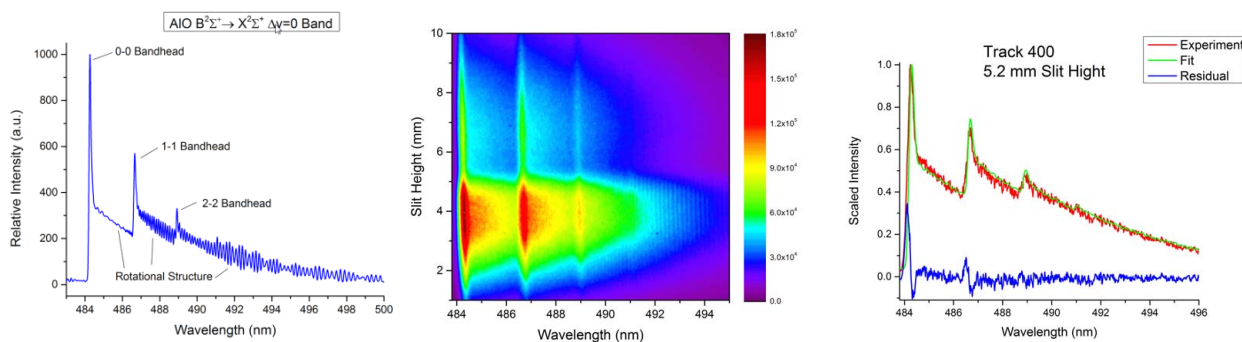


Figure 5. (Left) High-resolution AIO emission spectrum with an emission temperature of $T = 4000$ Kelvin and spectral resolution of $\Delta\lambda = 0.09$ nm. The spectrum is computed using tabulated AIO line strengths and the indicated parameters. (Middle) Recorded AIO emission spectra following laser-ablation of an aluminium sample; time delay 60 μs, gate width 6 μs. (Right) Fitted and recorded spectra for one track of the ICCD image, at a slight height of 5.2 mm.

from the Wigner-Witmer diatomic eigenfunctions [83], subsequently incorporating highly resolved diatomic molecular data together with extensive computations to diagonalize the Hamiltonians.

The temperature can be inferred from a diatomic emission spectrum. The details are elaborated here.

A diatomic band system typically consists of many vibrational bands each containing many rotational lines. This results in a regularity to the diatomic spectrum not seen in atomic spectra. This computable regularity in a diatomic spectrum offers some advantages to one designing a temperature diagnostic tool.

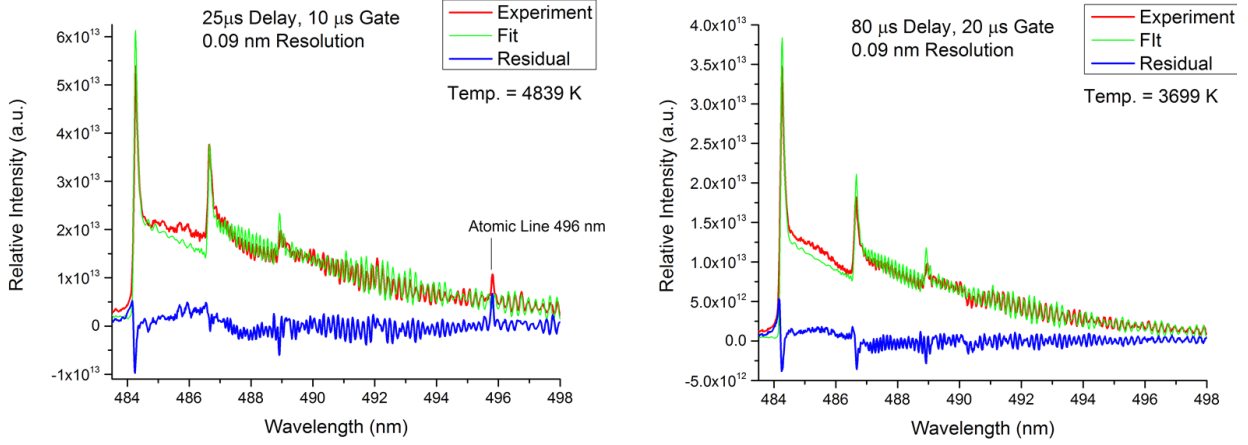


Figure 6. Fitted (green line) and measured (red line) high resolution AIO $B^2\Sigma^+ \rightarrow X^2\Sigma + \Delta v = 0$ spectra collected at 25 μs (Left) and 80 μs (Right) following optically induced breakdown. The inferred temperatures are 4839 and 3699 Kelvin, respectively.

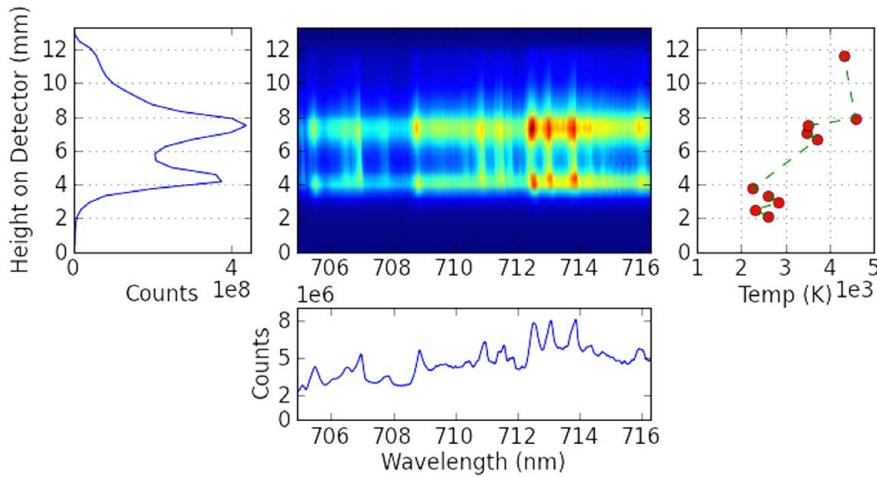


Figure 7. The image presents measured TiO spectra along the height of an ICCD detector for a time delay of 40 μs following optical breakdown, using a 2 μs window. In the above image, the sample surface is located near the 0 mm height on the detector, as the laser pulse was incident from the top. The plot to right of the image provides the temperature inferred from the TiO A-X system as function of height along the detector. The plot to the left and below the image represents the integrated intensity along the horizontal and vertical axes, respectively.

The equation for the intensity of a spectral line produced by free spontaneous emission can be written as

$$I_{ul} = h\nu_{ul}A_{ul}N_u. \quad (3)$$

Here, h is Planck's constant, ν_{ul} is frequency of the spectral line, A_{ul} is the Einstein transition probability (it is really the rate coefficient for transitions from upper level u to lower level l , and is often called

the Einstein A-coefficient), and N_u is the population density of upper level. A dimensional interpretation of Eq. (3) is that $h\nu_{ul}$ is the energy per photon, A_{ul} is number of photons radiated isotropically per second per excited state, and N_u is the number density of excited states. Although I_{ul} is often known by misnomer “intensity,” it is the rate at which energy is radiated isotropically per second per unit volume of gas. In thermal equilibrium, I_{ul}

can be written in terms of temperature T using Boltzmann factors,

$$I_{ul} = h\nu_{ul}A_{ul}\frac{N_0}{Q}e^{-E_u/kT}, \quad (4)$$

where N_0 denotes total population density, Q is the partition function, E_u is the energy eigenvalue of the upper state, and k is Boltzmann's constant. For a variety of reasons, relative rather than absolute values of intensity are recorded. Absolute intensity measurements are difficult and costly to perform. Even if absolute intensity measurements were recorded, the total population density N_0 is often only crudely known. Computation of the partition function Q is often tedious, and it would require that the temperature T be known. Finally, the relative values of the Einstein A-coefficients are often known with higher accuracy than absolute values. Thus, inference of temperature from diatomic spectra is almost invariably based on ratios of measured intensity. From a practical viewpoint, temperature determination from a recorded spectrum requires knowledge of the spectral sensitivity s_ν of the spectrometer-detector system, but not the absolute intensity calibration.

For the determination of temperature, many methods are based on recording the ratio of the intensities of two spectral lines or two vibrational bands. However, in the analysis of the spectra discussed in this work, the full recorded spectrum is used to infer temperature. The determination of the temperature is based on (a) fitting the entire spectrum, or (b) applying the so-called Boltzmann plot technique. The latter is based on the generation of semilog plots and subsequent determination of the slope to obtain a measure for temperature. The former is based on the computation of the entire spectrum by evaluating relative intensities to construct a synthetic spectrum for an assumed temperature T and a measured spectrometer bandpass function. A minimization algorithm such as the Nelder-Mead algorithm is found to work efficiently in finding the synthetic spectrum that best agrees with the recorded spectrum. Frequently, experimental spectra show a variable baseline offset that becomes another unknown parameter in the fitting process. Essential for the computation of the synthetic spectra is the so-called line strength S_{ul} , see Eq. (2).

References [84] and [85] show tables relating Einstein A-coefficients and the oscillator strength to the line strength.

Computation of a spectrum begins with specification of the spectral range λ_{\min} to λ_{\max} and the separation of this range into N wavelength bins corresponding to recorded detector pixels of width $\Delta\lambda$. The finite width of the spectrometer bandpass and also the modulation transfer function of the detector imply that each spectral line falling within the range λ_{\min} to λ_{\max} contributes intensity to several pixels. The tabulated line strengths are used to compute the contributions of each spectral line at each wavelength bin. The spectrometer's dispersion is not constant, therefore, the width $\Delta\lambda$ of a bin is actually a function of the wavelength, $\Delta\lambda_\lambda$.

The tabulated line strengths contain the required quantum mechanics for computation of a spectrum. We use line strengths obtained by fitting high-accuracy line position measurements to model Hamiltonians for the upper and lower states of the diatomic molecule. A subset of the computed term differences, *i.e.*, differences between upper and lower energy eigenvalues, represent actual spectral lines. Those term differences that correspond to allowed spectral lines are determined by computation of the Hönl-London factors. A spectral line is allowed if its Hönl-London factor is non-vanishing. This is the only diatomic selection rule we use. For a diatomic molecule, all angular momentum and parity selection rules follow from the non-vanishing of the angular momentum part of the transition moment, and the line strength is the square of the transition moment summed over all moments contributing to the same spectral line. Hamiltonian matrices are computed in the Hund case *a* basis. We use the Hund model as an exact mathematical basis with which to express the Wigner and Witmer [86, 87] diatomic eigenfunctions, but not to represent an approximate physical model. For the diatomic line strength, the Wigner-Witmer eigenfunction yields

$$S_{ul} = S_{n'v',nv}S_{J',J}, \quad (5)$$

where $S_{n'v',nv}$ is the electronic-vibrational strength that carries the units of line strength, and $S_{J',J}$ is the dimensionless Hönl-London or rotational line strength factor. The electronic-vibrational strength is further written in terms of Franck-Condon factors

and the so-called r-centroids [64]. For the computation of the electronic-vibrational strengths, the Born-Oppenheimer approximation is invoked, yet the calculation of vacuum wavenumbers and Hönl-London factors utilize the Wigner-Witmer diatomic eigenfunction but not the Born-Oppenheimer approximation.

4. DISCUSSION AND SUMMARY

In the laser-induced plasma experiments, a laser pulse is focused onto the sample surface of interest, or into gases and air. The radiation is absorbed after plasma generation, and as a result, radiation energy is transferred to the target material. In laser ablation, a crater is formed and material is removed partially from the interaction zone, but it also depends on the pulse duration and a transient liquid phase may exist. The lifetime of the plasma depends on the laser parameters, the condition of the surrounding gas and substance to be analysed. The temporal structure of the laser pulse has a decisive influence on the generated plasma and hence the emitted spectrum. Besides the temporal structure, incident irradiance, ambient gas pressure and type of gas affect the plasma dynamics. Time resolved diagnostics allow one to record atomic emission profiles separate from molecular recombination and/or excitation. However, atomic and molecular species can be measured simultaneously within a selected spectral window. By separating the events in time, one can determine the transient phenomena of the plasma. By separating the plasma evolution in space as well, one can evaluate both temporally- and spatially-resolved plasma dynamics.

Plasma in general emits and absorbs electromagnetic radiation with specific characteristics or fingerprints of emission spectrum. Laser induced Breakdown Spectroscopy (LIBS) experiments allow one in principle to develop a complete description of the plasma evolution in terms of kinetics of elementary processes such as collisional and radiative ionization/recombination, radiative processes, inverse bremsstrahlung and excitation/de-excitation due to electron impact processes. Collisional ionization has long range (*viz.* Coulomb force), intermediate (*viz.* induced dipoles) and short range (*viz.* neutral particles) interaction between electrons and ions, and neutral atoms and molecules.

Throughout the plasma generation and early decay, there will be a background continuum due to bremsstrahlung and recombination. This continuum decays with time at a faster rate than the spectral lines. In the bremsstrahlung process, electrons are accelerated or decelerated in collision process by emitting photons. The plasma is characterized by a variety of parameters including plasma temperature, electron density and degree of ionization. The plasma analysis can be accomplished using line shape characteristics, widths and shifts that are related to plasma temperature and electron density. Other techniques such as Rayleigh and Thomson scattering measurement can be applied as well to determine electron density. The atomic emission lines early in the laser-induced plasma dynamics for the hydrogen Balmer series lines such as H_α and H_β are primarily due to Stark broadening.

For nanosecond laser radiation, duration of the laser pulse is several orders of magnitude more than the characteristic lattice vibration time in a solid, and therefore heat transfer can be relatively fast compared with the characteristic time of the laser pulse. As the laser pulse progresses in time, the high electric field in the focal region of the laser begins to accelerate naturally present ions, plus ions formed via multi-photon or cascade interactions in the atmosphere above the sample, and from the sample itself. These free electrons increase the absorption of the laser radiation in the atmosphere above the sample, leading to greater multi-photon ionization and further absorption of the laser pulse. In general, more robust plasma will be formed by near-ir (≈ 1 eV) than near-uv (≈ 4 eV) and uv laser radiation due to favorable absorption characteristics.

5. CONCLUSION

Time resolved measurements of hydrogen- alpha, beta and gamma emissions allow one to characterize the plasma dynamics following optical breakdown. Stark widths and shifts can be used to determine electron density in the laser-induced plasma. The excitation temperature can be determined from Boltzmann plots. Analysis of molecular spectra allows one to evaluate plasma dynamics and onset of chemistry. Most important for future experimental studies will be measurements of highly resolved images that can be used to determine the spatial plasma dependencies and dynamics.

ACKNOWLEDGMENTS

The authors thank for support in part by the Center for Laser Application (CLA) at The University of Tennessee Space Institute (UTSI).

CONFLICT OF INTEREST STATEMENT

The authors confirm that there are no conflicts of interest with the presented work.

REFERENCES

1. L. J. Radziemski and D. A. Cremers (Eds.) 1989, *Laser-induced plasmas and applications*, M. Dekker, New York.
2. A. W. Miziolek, V. Palleschi and I. Schechter (Eds.) 2006, *Laser Induced Breakdown Spectroscopy*, Cambridge University Press, New York.
3. Cremers, D. A. and Radziemski, L. J. 2006, *Handbook of Laser-Induced Breakdown Spectroscopy*, John Wiley, New York.
4. J. P. Singh and S. N. Thakur (Eds.) 2007, *Laser Induced Breakdown Spectroscopy*, Elsevier Science, New York.
5. Noll, R. 2011, *Laser-Induced Breakdown Spectroscopy*, Springer, Heidelberg.
6. S. Musazzi and U. Perini (Eds.) 2014, *Laser-Induced Breakdown Spectroscopy*, Springer, Heidelberg.
7. Konjević, N. 1999, *Phys. Rep.*, 316, 339.
8. Aragón, C. and Aguilera, J. A. 2008, *Spectrochim. Acta Part B*, 63, 893.
9. Hahn, D. W. and Omenetto, N. 2010, *Appl. Spectrosc.*, 64, 335A.
10. Hahn, D. W. and Omenetto, N. 2012, *Appl. Spectrosc.*, 66, 347.
11. Anabitarte, F., Cobo, A. and Lopez-Higuera, J. M. 2012, *Int. Scholar. Res. Notic. (ISRN) Spectrosc.*, 2012, ID 28520.
12. Parigger, C. G. 2013, *Spectrochim. Acta Part B*, 79-80, 4.
13. De Giacomo, A., Dell'Aglio, M., De Pascale, O., Gaudiuso, R., Palleschi, V., Parigger, C. G. and Woods, A. C. 2014, *Spectrochim. Acta Part B*, 10, 180.
14. Gravel, J. F. Y. and Boudreau, D. 2009, *Spectrochim. Acta Part B*, 64, 56.
15. Brieschenk, S., O'Byrne, S. and Kleine, H. 2013, *Opt. Lett.*, 38, 664.
16. Brieschenk, S., Kleine, H. and O'Byrne, S. 2013, *J. Appl. Phys.*, 113, 103101.
17. Zuhlke, C. A., Bruce, J. III, Anderson, T. P., Alexander, D. R. and Parigger, C. G. 2014, *Appl. Spectrosc.*, 68, 1021.
18. Ochkin, V. N. 2008, *Spectroscopy of Low Temperature Plasma*, Wiley-VCH, Weinheim.
19. Kunze, H. J. 2009, *Introduction to Plasma Spectroscopy*, Springer Ser. Atom, Opt., Plasm. Phys., Berlin.
20. Devdariani, A. (Ed.) 2012, *21st International Conference on Spectral Line Shapes*, J. Phys.: Conf. Ser., 397, Institute of Physics (IOP) Publishing, Bristol.
21. Parigger, C. G. (Ed.) 2014, *22nd International Conference on Spectral Line Shapes*, J. Phys.: Conf. Ser., 548, Institute of Physics (IOP) Publishing, Bristol.
22. Yang, C. S. C., Brown, E. E., Hommerich, U. H., Trivedi, S. B., Samuels, A. C. and Snyder, A. P. 2007, *Appl. Spectrosc.*, 61, 321.
23. Mao, X., Bol'shakov, A. A., Choi I., McKay, C. P., Perry, D. L., Sorkhabi, O. and Russo, R. E. 2011, *Spectrochim. Acta Part B*, 66, 767.
24. Parigger, C. G., Woods, A. C. and Hornkohl, J. O. 2012, *Appl. Opt.* 51, B1.
25. Parigger, C. G., Woods, A. C., Keszler, A., Nemes, L. and Hornkohl, J. O. 2012, *American Institute of Physics (AIP) Conf. Proc.*, 1464, 628.
26. Parigger, C. G., Woods, A. C. and Rezaee, M. R. 2012, *J. Phys.: Conf. Ser.*, 397, 012022.
27. Pardini, L., Legnaioli, S., Lorenzetti, G., Palleschi, V., Gaudiuso, R., De Giacomo, A., Dias Pace, D. M., Anabitarte Garcia, F., de Holanda Cavalcanti, G. and Parigger, C. G. 2013, *Spectrochim. Acta Part B*, 88, 98.
28. Parigger, C. G., Woods, A. C., Witte, M. J., Swafford, L. D. and Surmick, D. M. 2014, *J. Vis. Exp.*, 84, E51250.
29. Surmick, D. M. and Parigger, C. G. 2014, *Appl. Spectrosc.*, 68, 992.
30. Swafford, L. D. and Parigger, C. G. 2014, *Appl. Spectrosc.*, 68, 1016.
31. Parigger, C. G., Woods, A. C., Surmick, D. M., Swafford, L. D. and Witte, M. J. 2014, *Spectrochim. Acta Part B*, 99, 15.
32. Parigger, C. G., Swafford, L. D., Woods, A. C., Surmick, D. M. and Witte, M. J. 2014, *Spectrochim. Acta Part B*, 99, 28.
33. Parigger, C. G., Woods, A. C., Surmick, A. B., Donaldson, A. B. and Height, J. L. 2014, *Appl. Spectrosc.*, 68, 362.

34. Witte, M. J., Parigger, C. G., Bullock, N. A., Merten J. A. and Allen S. D. 2014, *Appl. Spectrosc.*, 68, 367.
35. Hornkohl, J. O., Woods, A. C. and Parigger, C. G. 2014, *J. Phys.: Conf. Ser.*, 548, 012033.
36. Woods, A. C. and Parigger, C. G. 2014, *J. Phys.: Conf. Ser.*, 548, 012037.
37. Hornkohl, J. O., Fleischmann, J. P., Surmick, D. M., Witte, M. J., Swafford, L. D., Woods, A. C. and Parigger, C. G. 2014, *J. Phys.: Conf. Ser.*, 548, 012040.
38. Parigger, C. G., Swafford, L. D., Surmick, D. M., Witte, M. J., Woods, A. C. and Gautam, G. 2014, *J. Phys.: Conf. Ser.*, 548, 012043.
39. Swafford, L. D., Surmick, D. M., Witte, M. J., Woods, A. C., Gautam, G. and Parigger, C. G. 2014, *J. Phys.: Conf. Ser.*, 548, 012049.
40. Witte, M. J. and Parigger, C. G. 2014, *J. Phys.: Conf. Ser.*, 548, 012052.
41. Woods, A. C. and Parigger, C. G. 2014, *J. Phys.: Conf. Ser.*, 548, 012053.
42. Gornushkin, I. B., Merk, S., Demidov, A., Panne, U., Shabanov, S. V., Smith, B. W. and Omenetto, N. 2012, *Spectrochim. Acta B*, 76, 203.
43. Buckley, S. 2014, *Spectrosc.*, 29, 22.
44. Parigger, C. G., Hornkohl, J. O. and Nemes, L. 2010, *Int. J. Spectrosc.*, 2010, ID 593820.
45. Merten, J., Jones, M., Shepherd, C., Parigger, C. G. and Allen, S. D. 2014, *Proc. Society of Photo-Optical Instrumentation Engineers (SPIE)*, 8710, 87100S.
46. Johnson, J. B., Allen, S. D., Merten, J., Johnson, L., Pinkham, D. and Reeve, S.W. 2014, *J. Spectrosc.*, 2014, ID 613435.
47. Merten, J., Jones, M., Hoke, S. and Allen, S. D. 2014, *J. Phys.: Conf. Ser.*, 548, 012042.
48. Unnikrishnan, V. K., Choudhari, K. S., Kulkarni, S. D., Nayak, R., Kartha, V. B., Santhosh, C. and Suri, B. M. 2014, *Pramana J. Phys.*, 82, 397.
49. Pathak, A. K., Rai, N. K., Singh, A., Rai, A. K. and Rai, P. K. 2014, *J. Phys.: Conf. Ser.*, 584, 012007.
50. Splinter, R. and Parigger, C. G. 2015, Fluid dynamics phenomena in cardiovascular ablation with laser radiation, in: *Lasers in Cardiovascular Interventions*, O. Topaz (Ed.), Springer, New York.
51. Noack, J. and Vogel, A. 1999, *Inst. of Electrical and Electronics Engineers (IEEE), J. Quant. Electron.*, 35, 1156.
52. Cowan, R. D. and Dieke, G. H. 1948, *Rev. Mod. Phys.*, 20, 418.
53. Parigger, C. G., Plemmons, D. H. and Oks, E. 2003, *Appl. Opt.*, 42, 5992.
54. Konjević, N., Ivković, M. and Sakan, N. 2012, *Spectrochim. Acta Part B*, 76, 593.
55. Kielkopf, J. F. and Allard, N. F. 2014, *J. Phys. B: At. Mol. Opt. Phys.*, 47, 1.
56. Konjević, N., Lesage, A., Fuhr, J. R. and Wiese, W. L. 2002, *J. Phys. Chem. Ref. Data*, 31, 819.
57. Moon, H., Herrera, K. K., Omenetto, N., Smith, B. W. and Winefordner, J. D. 2009, *Spectrochim. Acta Part B*, 64, 702.
58. Omenetto, N., Winefordner, J. D. and Alkemade, C. Th. J. 1975, *Spectrochim. Acta*, 30B, 335.
59. Bulajic, D., Corsi M., Cristoforetti, G., Legnaioli, S., Palleschi, V., Salvetti, A. and Tognoni, E. 2002, *Spectrochim. Acta Part B*, 57, 339.
60. El Sherbini, A. M., El Sherbini, Th. M., Hegazy, H., Cristoforetti, G., Legnaioli, S., Palleschi, V., Pardini, L., Salvetti, A. and Tognoni, E. 2005, *Spectrochim. Acta Part B*, 60, 1573.
61. El Sherbini, A. M., Hegazy, H. and El Sherbini, Th. M. 2006, *Spectrochim. Acta Part B*, 61, 532.
62. Du, Y., Ding, Y., Liu, Y., Lan, L. and Peng, Z. 2014, *Appl. Opt.*, 53, 4922.
63. Hornkohl, J. O., Parigger, C. G. and Nemes, L. 2006, *Appl. Opt.*, 44, 3686.
64. Hornkohl, J. O., Nemes, L. and Parigger, C. G. 2011, *Spectroscopy of Carbon Containing Diatomic Molecules*, in: *Spectroscopy, Dynamics and Molecular Theory of Carbon Plasmas and Vapors*, L. Nemes and S. Irlé (Eds.), World Scientific Publishing, Singapore.
65. Chen, C. S., Man, B. Y., Liu, D., Song, X. and Chen, X. J. 2013, *J. Phys. B.*, 46, 015701.
66. Hermann, J., Thomann, A. L., Boulmer-Leborgne, C., Dubreuil, B., De Giorgi, M. L., Perrone, A., Luches, A. and Mihailescu, I. N. 1995, *J. Appl. Phys.*, 77, 2928.
67. De Giacomo, A., Dell'Aglio, M., Santagata, A. and Teghil, R. 2005, *Spectrochim. Acta, Part B*, 60, 935.
68. Woods, A. C., Parigger, C. G. and Hornkohl, J. O. 2012. *Opt. Lett.*, 37, 5139.

-
69. Woods, A. C., Parigger, C. G. and Hornkohl, J. O. 2012, *Int. Rev. Atom. Mol. Phys.*, 3, 103.
70. Willmott, P. R. and Huber, J. R. 2000, *Rev. Mod. Phys.*, 72, 315.
71. Giacomo, A. D., Shakhmatov, V., Senesi, G., Pascale, O. D. and Prudenzano, F. 2002, *Appl. Surf. Sci.*, 186, 533.
72. Yalçın, Ş., Crosley, D., Smith, G. and Faris, G. W. 1999, *Appl. Phys. B*, 68, 121.
73. Ciucci, A., Corsi, M., Palleschi, V., Rastelli, S., Salvetti, A. and Tognoni, E. 1999, *Appl. Spectrosc.*, 53, 960.
74. Capitelli, F., Colao, F., Provenzano, M. R., Fantoni, R., Brunetti, G. and Senesi, N. 2002, *Geoderma*, 106, 45.
75. Semaltianos, N. G., Logothetidis, S., Frangis, N., Tsiaoussis, I., Perrie, W., Dearden, G. and Watkins, K. G. 2010, *Chem. Phys. Lett.*, 496, 113.
76. Assim, E. M. 2008, *J. Alloys Compd.*, 465, 1.
77. Linsebigler, A. L., Lu, G. and Yates, J. T. 1995, *Chem. Rev.*, 95, 735.
78. Ollis, D. F. 2000, *Comptes Rendus de l'Académie des Sciences-Series IIC-Chemistry*, 3, 405.
79. O'Regan, B. and Grätzel, M. 1991, *Nature*, 335, 737.
80. Grant, C. D., Schwartzberg, A. M., Smestad, G. P., Kowalik, J., Tolbert, L. M. and Zhang, J. Z. 2002, *J. Electroanal. Chem.*, 522, 40.
81. Danehy, P. M., Bathe, B. F., Johansen, C. T., Cutler, A. D. and Hurley, S. 2014, *Von Karman Inst. (VKI) Lect. Ser. Spectroscopy and Spectroscopic Measurement Techniques for Aerospace Flows* (Brussels, May 9 - 17, 2014) ID 20140006405.
82. Couris, S., Kotzagianni, M., Baskevicius, A., Bartulevicius, T. and Sirutkaitis, V. 2014, *J. Phys.: Conf. Ser.*, 548, 012056.
83. Hornkohl, J. O., Woods, A. C. and Parigger, C. G. 2014, *J. Appl. Laser Spectrosc.*, 1, 13.
84. Thorne, A. 2013, *Spectrophysics*, 2nd Ed., Chapman and Hall, London.
85. Hilborn, R. C. 1982, *Am. J. Phys.*, 50, 982.
86. Wigner, E. and Witmer, E. E. 1928, *Z. Phys.*, 51, 859.
87. Hettema, H. 2000, *Quantum Chemistry: Classic Scientific Papers*, World Scientific, Singapore.